SPHERE IFS: the spectro differential imager of the VLT for Exoplanets search

R.U. Claudi [*a], M. Turatto [b], E. Giro [a], D. Mesa [a], U. Anselmi [a], P. Bruno [b], E. Cascone [c], V. De Caprio [d], S. Desidera [a], R. Dorn [e], D. Fantinel [a], G. Finger [e], R. G. Gratton [a], L. Lessio [a], J.L. Lizon [e], B.Salasnic [a], S. Scuderi [b], K. Dohlen [f], J. L. Beuzit [g], P. Puget [g], J. Antichi [g], N. Hubin [e], M. Kasper [e]

[a] INAF – Osservatorio Astronomico di Padova, Vicolo dell'Osservatorio 5, Padova, ITALY, 35122-I
[b] INAF – Osservatorio Astrofisico di Catania, Via S.Sofia 78, Catania, ITALY, 95123-I
[c] INAF – Osservatorio Astronomico di Capodimonte, Salita Moiariello, 16, ITALY, 80131-I
[d] INAF – IASF sezione di Milano, Via E. Bassini 15, Milano ITALY, 20133-I
[e] ESO,European Southern Observatory (ESO), Karl-Schwarzschild-Str.2, 85748 Garching, Germany
[f] Laboratoire d'Astrophysique de Marseille, B.P. 8, F-13376 Marseille Cedex 12, France
[g] Laboratoire d'Astrophysique de l'Observatoire de Grenoble, Rue de la Piscine 414, Saint-Martin d'Hères, France, 38400-F

ABSTRACT

The SPHERE is an exo-solar planet imager, which goal is to detect giant exo-solar planets in the vicinity of bright stars and to characterize them through spectroscopic and polarimetric observations. It is a complete system with a core made of an extreme-Adaptive Optics (AO) wavefront correction, a pupil tracker and diffraction suppression through a variety of coronagraphs. At its back end, a differential dual imaging camera and an integral field spectrograph (IFS) work in the Near Infrared (NIR) Y, J, H and Ks bands (0.95 – 2.32μm), and a high resolution polarization camera covers the optical range (0.6 – 0.9 μm). The IFS is a low resolution spectrograph (R~50) working in the near IR (0.95-1.65 microns), an ideal wavelength range for the detection of giant planet features. In our baseline design the IFU is a new philosophy microlens array of about 145x145 elements designed to reduce as much as possible the cross talk when working at diffraction limit. The IFU will cover a field of view of about 1.7 x 1.7 square arcsecs reaching a contrast of 10^{-7}, providing a high contrast and high spatial resolution "imager" able to search for planet well inside the star PSF.

Keywords: Integral Field Spectrograph, Exo Planets, Spectroscopy; High Contrast imaging

1. INTRODUCTION

SPHERE (Spectro-Polarimetric High-contrast Exoplanets Research) is a second generation instrument for VLT optimized for high contrast imaging at the Nasmyth focus of one of the VLT units. SPHERE is made of four subsystems: the Common Path Optics and three science channels, a differential imaging camera (IRDIS), an Integral Field Spectrograph (IFS), and a visible imaging polarimeter (ZIMPOL). The Common Path includes pupil stabilizing fore optics (tip-tilt and derotator) where insertable polarimetric half-wave plates are also provided, the SAXO extreme adaptive optics system with a visible wavefront sensor, and NIR coronagraphic devices in order to feed IRDIS and IFS with a highly stable coronagraphic image in the NIR. IFS explores the stellar neighbourhood in order to find planetary spectral features. For the IFS, this quest is conducted searching for strong CH_4 absorption bands in both the stellar light reflected by gaseous Jupiter-like planets and in thermal emission from young-warm planets. Moreover it will be possible to have a first order characterization of the low mass companion itself. Additional science topics which will be addressed by SPHERE include the study of brown dwarfs, circumstellar disks and related phenomena such as mass loss mechanisms, stellar winds, planetary nebulae and perhaps even supernova explosions.

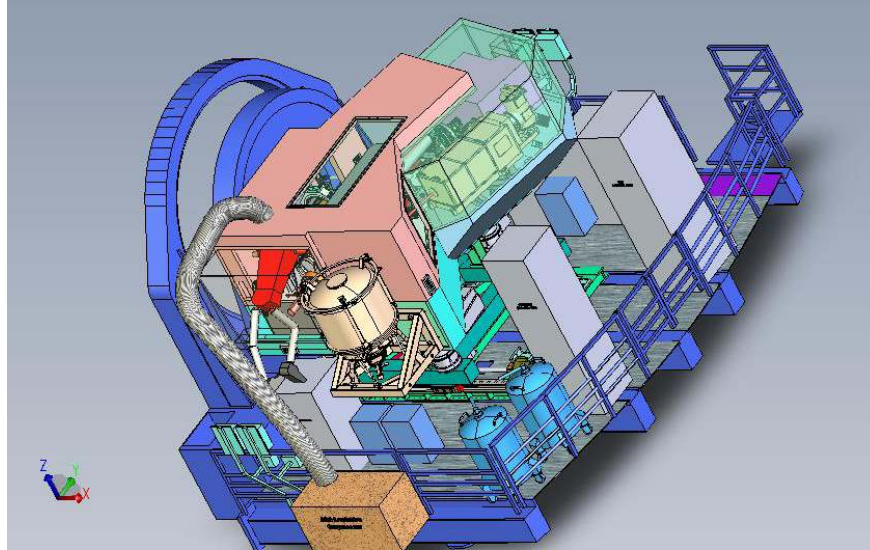The Optomechanical design of SPHERE is shown in Figure 1.

Figure 1:Mechanical Layout of the whole SPHERE. The instrument will fill the Nasmyth room of the VLT. In transparence is possible to see the IFS.

2. IFS: OVERVIEW AND STATUS REPORT

The basic characteristic of an IFS is to image the array of slits generated by an Integral Field Unit (IFU) and chromatically separated by a suitable dispersing device on the final image plane. Once chromatically dispersed, the final Exit Slits form then the array of spectra of an Integral Field Spectrograph.

2.1 Optomechanics

The heart of IFS is a new kind of lens-based IFU called BIGRE[1](see Paragraph 2.2). Specifically, BIGRE is placed at the interface of the instrument with the SPHERE Common Path (CP) and it is optically conjugated with the telescope Focal Plane, this latter being re-imaged by an F/# = 316 beam. This allows to sample the diffractive PSF - arising from the AO compensation and the Coronagraphic spatial filtering, working both inside the CP optics - at the Nyquist's limit[2]. The purpose of this instrument is thus to realize diffraction limited Integral Field Spectroscopy with the high-contrast capabilities of the BIGRE device as IFU. To this scope, the whole IFS system, which is downstream the entrance slits array should only re-image and disperse these slits with the highest optical stability and a good optical quality. To achieve[1] this goal, the optimized IFS optical design is a fully dioptric concept design, shaped by several optics located along a straight optical axis. IFS is projected to work, with different resolution in two different wavelength ranges: with a resolution of R~50 in the 0.95-1.35 μm (z-J mode) while a lower resolution (R~30) is considered for the wider wavelength range of 0.95 – 1.65 μm (z-J-H mode). The two different resolutions are achieved by two different Amici prisms. The two working wavelength ranges are defined by a combination of band pass, high pass and low pass filter mounted in two locations: inside the dewar (low pass filter) and just in front of prisms (band pass filter for the z-J mode and high pass filter for the z-J-H mode).

From a general point of view the IFS is composed of several main sub-systems (see Figure 2):

- the IFU

- the Collimator

- a filter wheel with several neutral density filters limiting the flux received by the IR detector during the FF calibration

- a prism slide to select between the two different prisms

- a camera mounted on a focusing slide and a piezoelectric slide for dithering

- a 2K $\times$ 2K Hawaii 2RG IR Detector with pixel of 18.0 µm working in the wavelength range 0.95 – 2.32 µm.
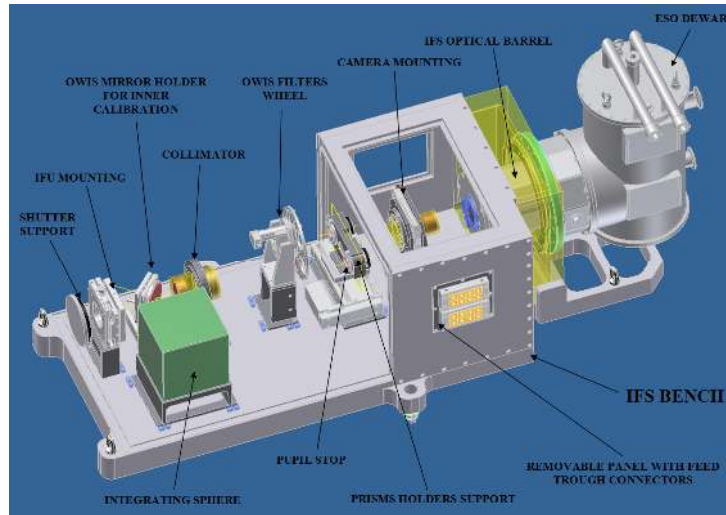

Figure 2: The IFS mechanical Layout

Further, there are also several ancillary sub-systems:

- an internal Calibration Arm constituted by several light sources feeding an integrating sphere. The output of the integrating sphere is folded by a pick up mirror in order to illuminate the detector

- a cryostat housing the IR Detector

2.2 BIGRE

BIGRE is a new scheme for the integral field unit based on a dual-lenslet device (see Figure 3), that solves some of the problems related to the classical single lenslet (TIGER) design when used for such applications. BIGRE provides much lower cross-talk signals than TIGER, allowing a more efficient use of the detector pixels and a considerable saving of the overall cost of a lenslet-based integral field spectrograph.
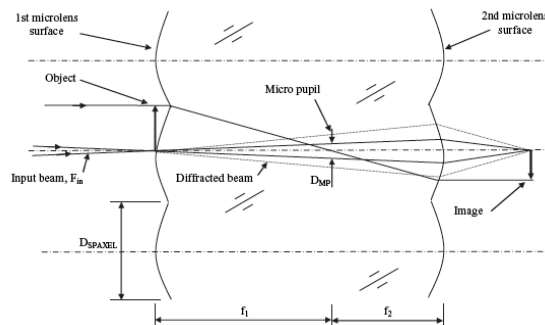

Figure 3: Scheme of a BIGRE (see text)

Figure 3 shows a BIGRE spaxel working at the diffraction limit with an un-resolved entrance pupil. The first lens lies on a focal plane and reimages a micropupil at its focal distance (f_1). The electric field imaged onto this optical plane is a sinc function (one dimension) or a Jinc function (two dimensions). This signal is filtered by a top-hat transmission function

and finally reimaged onto an image plane by the second lens. The distance between this intermediate pupil plane and the second lens is its focal length (f_2). The electric field imaged by this second lens is an un-bound signal with upper envelope much steeper than the one proper to a sinc profile (u^{-1}) or a Jinc profile ($u^{-1.5}$). A complete description of the BIGRE theory could be found in Antichi et al. (2009)[1].

2.3 Control Electronics

The control electronics design is realized considering the standard specifications of ESO. All the controlled functions are standardized as much as possible, and a modular approach to the design facilitates the maintenance and improves the reliability of the instrument. With reference to Figure 2, the IFS controlled functions are: the Calibration mirror located just in front of the Integrating Sphere, a Filter Wheel in between the collimator and the Camera, just in front of the camera there is the disperser slide for the prism selection. The camera is mounted on a translation slide in order to focalize it and on a X-Y piezo stage for Flat fielding chopping. Other control electronics are the controller of the detector: NGC (fro ESO) and the Jumo Cryo Controller. In Figure 4 an overview of the instrument control hardware is given.
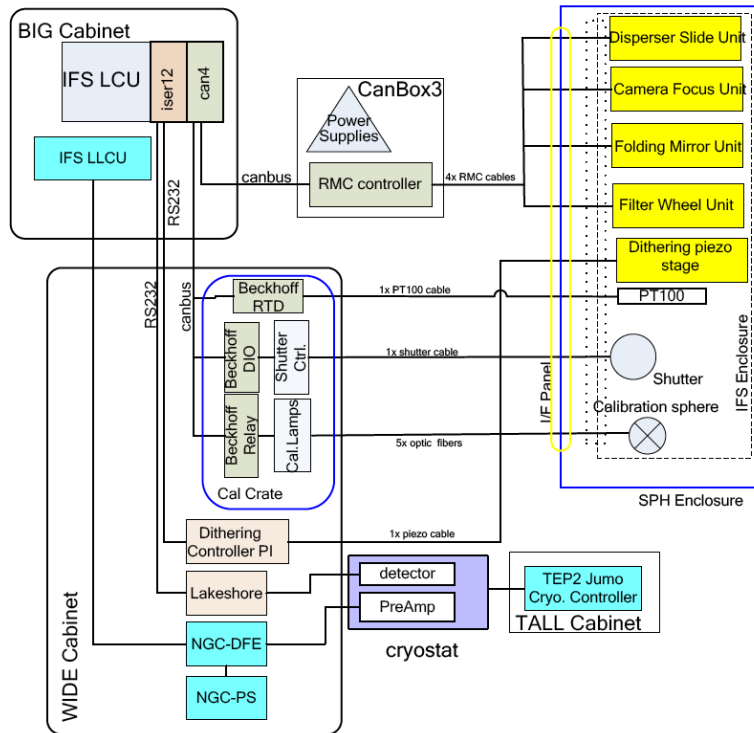

Figure 4: Overview of the IFS Instrument Control Hardware Architecture.

3. THE DETECTOR AND THE DEWAR

The detector of the IFS is a 2k×2k Hawaii 2RG array manufactured by Teledyne Imaging Sensors. The detector will be operated with cryogenic preamplifiers located next to the focal plane at temperatures of ~80 K. Both the Detector and the IFS dewar are shown in Figure 5.

The data acquisition system is the new NGC controller by ESO. The controller reads all the 32 video channels of each of the two Hawaii-2RG detectors in parallel. The H2RG detectors will be delivered with the CdZnTe substrate removed. This is now the standard array structure delivered by Teledyne. It potentially offers higher quantum efficiency at shorter wavelengths. It is also less affected by cosmic rays, which contaminate long exposures.
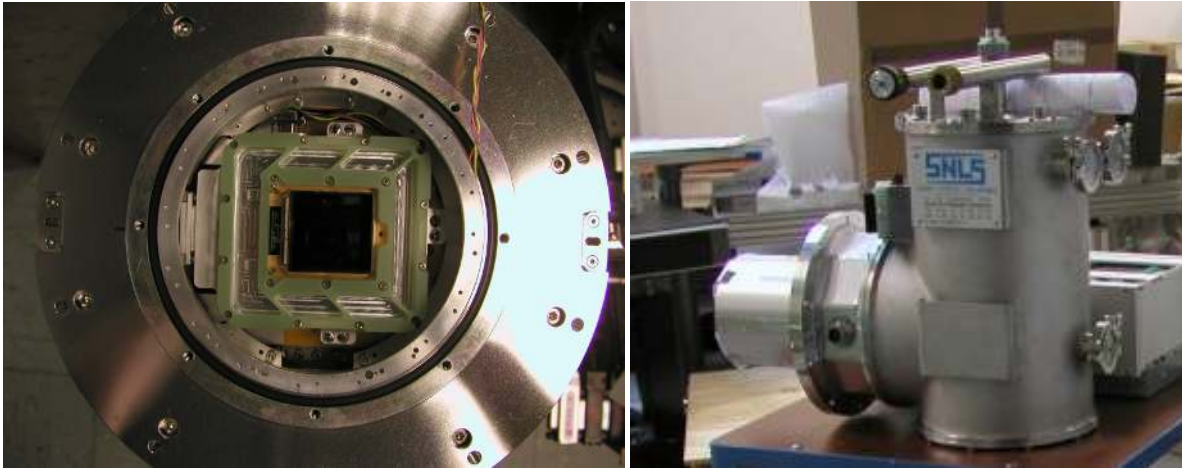
Figure 5: The 2k×2k Hawaii2RG array inside the IFS Dewar and on the right the IFS dewar

Science detector has been evaluated and show excellent noise performance at the nominal operation temperature of ~80 K (see Figure 6). Read noise as low as 8 electrons for a normal double correlated read and down to 3 electrons for non destructive sampling have been measured.
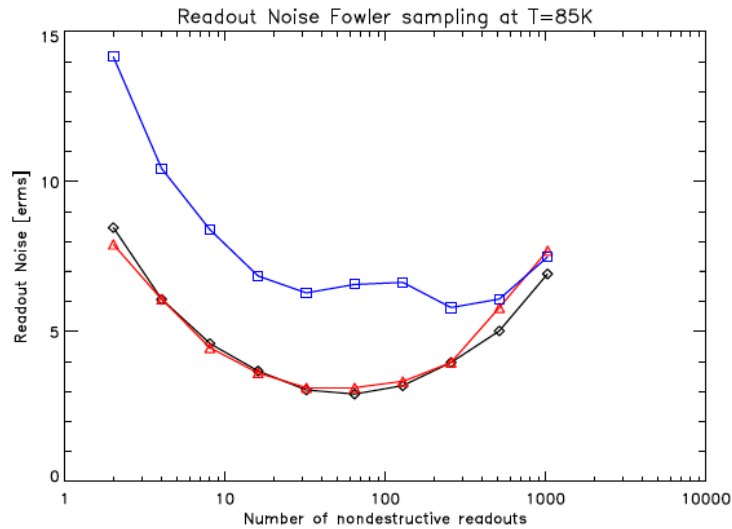

Figure 6: Measured noise for SPHERE detectors. The red curve is the measured noise for the IFS detector

Moreover the detector has high quantum efficiency over a broad band peaking from 96 to 100 % in J- Band, 96 to 97 % in H-Band and 86 to 89% in K-Band (see Figure 7). Interpixel coupling has been reduced compared to previous H2RGs tested at ESO with a maximum coupling of about 2% to the neighboring pixels. The conversion gain has been InterPixel capacitance corrected and it is (1.8698 ± 0.009) e$^-$/ADU.

The cosmetic quality of the detector fulfills the specifications for science grade device, if it has some hot pixels but no cluster of bad pixels spread over the array.

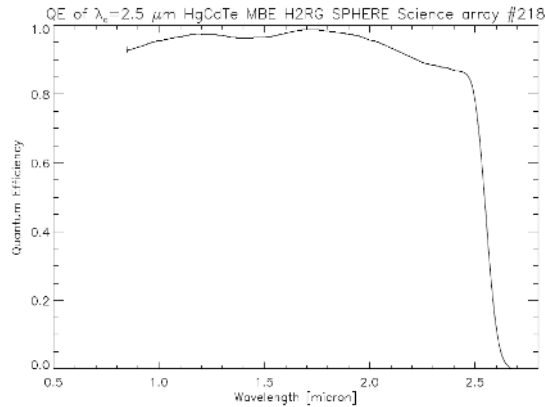Dark current is low: (2.46 ± 0.02) e$^-$/s and will allow a read noise limited detector performance in Sphere.

Figure 7: measured quantum efficency for the IFS detector.

Latent charge, or "persistence", is the remaining signal apparent in a series of dark exposures, after the array has been exposed to a bright radiation source. Any process which, after some delay, releases charge into the conduction band can contribute to latent charge. Latent charge is a function of photon flux during a previous exposure and the time elapsed since the previous exposure. The IFS detector shows little persistence at working temperature (~80e⁻).

4. SPECKLE SUBTRACTION THROUGH DIFFERENTIAL IMAGING

The dominant noise contributions for high contrast imaging instruments are due to the stellar background. Coronagraphy represents the first remedy, attenuating the coherent diffraction pattern of the on-axis PSF. At very high SR levels, the diffraction pattern dominates much of the on-axis PSF and coronagraphy can achieve strong attenuation with respect to off-axis signals whose direction is contained in the isoplanatic angle. However, with the SR levels obtained from ground by the present XAO devices, the coronagraphic efficiency is limited by the presence of a rapidly changing halo of Speckles generated by phase distortions at the level of the telescope Entrance Pupil. In addition, phase aberrations inside the optical train - not corrected by AO - produced for example by temporal variations of the optical alignment, or by different optical paths in a frozen optical alignment (hereafter non-common path aberrations), produce speckles (hereafter super-speckles) of a much longer lifetime than the ones produced by the atmospheric turbulence. Speckles and super-speckles are the major sources of noise for high contrast imaging instruments equipped with XAO-devices.

Three main techniques have been developed to reduce the impact of speckles in high contrast imaging: Angular Differential Imaging (ADI), simultaneous Spectral Differential Imaging (SDI) and Speckle Deconvolution (SD).

ADI[3] is a Point Spread Function (PSF) calibration technique that consists of the acquisition of a sequence of images with an altitude/azimuth telescope and the instrument rotator turned off (at the Cassegrain focus) or adjusted (Nasmyth) to keep the instrument and telescope optics aligned. This setup improves the stability of the quasi-static PSF structure throughout the sequence, while it causes a slow rotation of the field of view (FOV) with respect to the instrument. Note that only the FOV, not the PSF, rotates with time. Since the FOV rotates during an exposure, companion PSFs are smeared azimuthally. Let us now assume aberrations which are static with respect to the pupil, while field rotates. In this case it is not only possible to reduce the noise due to static speckles because different independent background speckles are sampled while the planet image moves with respect to the fixed speckle pattern (which would give a square root reduction factor), but rather directly subtract them by simply assuming that the speckle pattern measured in two epochs, one when the planet was in a location, and the other when the planet is not anymore there, are identical. ADI can be applied both to monochromatic and spectroscopic images and at least in principle together with other techniques. However, it requires that the arc covered by the companion is longer than the image size. The fastest the arc is covered, the best ADI works. For this reason, ADI is most successful at relatively large separations from the central star. A very successful code based on the ADI concept is LOCI[4].

The fundamental SDI step is the simultaneous image acquisition at adjacent wavelengths in a spectral range where the planetary and stellar spectra differ appreciably. From ground-based observations, the wavelength range 0.95-1.65 μm is

well suited for EGPs having atmospheric temperatures T <1500 K; while the K-band is indicated only for the warmest EGPs class, with atmospheric temperature T >1500 K. Let be $S(\lambda,\theta)$ the monochromatic spectral signal corresponding to a fixed sky angular position (θ) in the FOV. This can be expressed as the sum of the spectral signal of the star: $s(\lambda,\theta)$, and the spectral signal of a candidate low-mass companion candidate (or EGP) which lies specifically in this angular position: $p(\lambda,\theta)$. Fixing a wavelength range $[\lambda_1-\lambda_2]$, the following relations hold:

$S_1(\lambda_1,\theta) = s(\lambda_1,\theta) + p(\lambda_1,\theta)$

$S_1(\lambda_2,\theta) = s(\lambda_2,\theta) + p(\lambda_2,\theta)$

The basic SDI assumption is that after suitable flux normalization and chromatic re-scaling, the following relations hold for the boundary wavelengths of the range above:

$p(\lambda_2,\theta) = 0$

$s(\lambda_1,\theta) = s(\lambda_2,\theta)$

Then, the difference between $S(\lambda_1,\theta)$ and $S(\lambda_2,\theta)$ should return - in principle - the spectral signal $p(\lambda_1)$ only, i.e. the one proper to the low-mass (or EGP) candidate. The main difference between the SDI (as applied in NACO-SDI or IRDIS at SPHERE) and a true Spectroscopic-SDI calibration technique lies on the definition of the wavelength λ_1 and λ_2. For the SDI calibration technique, λ_1 and λ_2 represent the central wavelengths of two narrow-band chromatic filters, which bandwidths are $\Delta\lambda_1$ and $\Delta\lambda_2$. Instead, for Spectroscopic-SDI λ_1 and λ_2 are properly selected wavelengths, and the range $[\lambda_1-\lambda_2]$ represents the step by which a suitable disperser samples spectrally the total signal $S(\lambda,\theta)$. The direct advantage lies in the possibility to have very low levels of differential aberration allowing very accurate image subtractions. While working with narrow-band filters, a number of precautions are required because non-common path static aberrations represent a pathology which severely limits the performances of standard SDI instrumentation in obtaining the high contrast imaging regimes suitable for the EGPs direct detection.

The request of a calibration technique more efficient than SDI but still based on the simultaneous difference of chromatic images of the same target field was already suggested by Marois et al.[5,6], which showed than that the speckle noise reduction could be much more efficient if observations at three wavelength were available using their so called Double Difference method. Starting from there, it is reasonable to assume that a larger number of images at different wavelengths, taken with a small regular spectral step, can result in even better reduction of Speckle Noise with true Spectroscopic-SDI calibration technique. This thought suggests the use of Integral Field Spectroscopy for collecting data simultaneously at a large number of different wavelengths, given by the total spectral length and the spectral Resolution of a suitable Disperser. Specifically, the purpose of Integral Field Spectroscopy for the direct detection of extrasolar planets - then working in diffraction limited condition - is to exploit the spectral features of the sub-stellar companions (e.g. an extrasolar planet) in order to increase the contrast on the stellar background and then to exploit the Spectroscopic-SDI calibration technique for attenuating the Speckle Noise down to the level of the photon noise, cfr. Berton et al.[2].

While the SDI can be applied over the whole FoV, its main disadvantage is that it can only provide differential fluxes, and should then assume a planet spectrum. Furthermore, wavelength dependence of speckles[7] is only approximately taken into account, leaving uncorrected residuals.

Thatte et al.[8] proposed a different way to look at the data cube, that is called Speckle Deconvolution; this method may be considered as an extension of the double difference imaging of Marois et al.[5], but it has the merit to better emphasize regularities of the speckle pattern (see also Sparks & Ford[7]). The principle of the method is that speckles are expected to change regularly with wavelength. After appropriate radial scaling of the monochromatic images (proportionally to the wavelength λ), spectra for each spaxel should be well reproduced by a smooth function, which is represented by a low order polynomial in $(1/\lambda)$. If such polynomials are then subtracted, and the images are rescaled back, the resulting data-cube should result clean of speckles. However, as x illustrates, some residuals are still present in realistic simulations; for the SPHERE simulations, residuals with respect to a low order polynomial in $(1/\lambda)$ are of the order of a few per cent; since some ~30 spectral points are used, the expected improvement using this method is of ~100 over the monochromatic coronagraphic images.
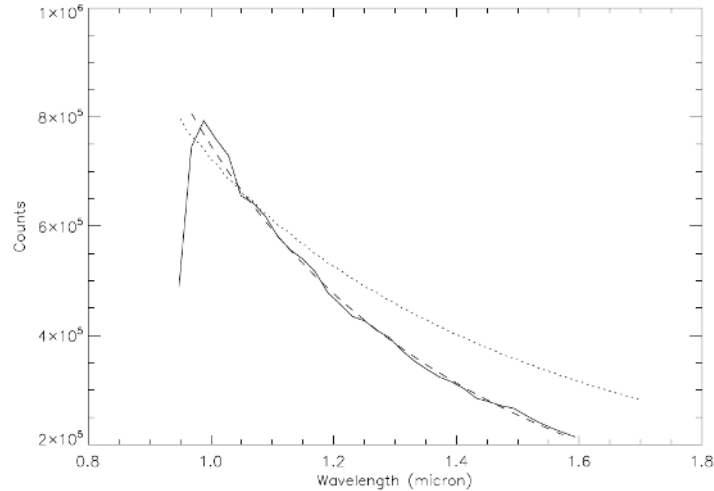
Figure 8: Example of the simulated spectrum on a spaxel re-scaled according to wavelength for SPHERE IFS according to our simulations. The dotted line is the spectrum entering the IFS. The solid line is the spectrum as measured on the IFS detector (after appropriate data reduction). Note that in the second case the run of the spectrum is not perfectly smooth. The dashed line is a fit to the solid line with a polynome in $1/\lambda$.

The method to work properly, it should be possible to clean the image from the planet image. In the scaled images, the radial location of the planet images changes proportionally to wavelength. Outside a given separation (bifurcation point), speckle pattern at a given wavelength can be reconstructed (and eliminated) using regions unaffected by the planet image. Inside the bifurcation point a (less reliable) iterative procedure is required, which makes some assumption about the shape of the speckle pattern to be subtracted. The radial coordinate r of the bifurcation point is given by:

$$r = 2\ \varepsilon\ 1.22\ (\lambda_0/D)\ [\lambda_1 / (\lambda_2 - \lambda_1)],$$

where λ_1 and λ_2 are the minimum and maximum wavelength of the IFS spectra (0.95 and 1.35 μm), λ_0 an intermediate value, D the telescope diameter, and ε a suitable parameter related to the "inclination" of the spectra of the planet within the data cube in the scaled images: ε=1 corresponds to the situation in which at a given scaled radial distance, there is no spectral region clean from the planet image (but just so). If ε>1 there is some part of the scaled image free from the planet signature, that can be used to reconstruct the speckle profile. The bifurcation point for the SPHERE-IFS is at about 0.20 arcsec for the Y-J mode, and at about 0.12 arcsec for the Y-H mode, which corresponds to about 7-8 λ/D in the first case, and 4-5 λ/D in the second one. This last is only slightly larger than the Inner Working Angle of the Coronagraph. This procedure can then be safely applied over most of the field of view of the SPHERE-IFS.

The main advantage of SD is that it directly provides the spectrum of the faint companion, with no assumption about its shape. On the other hand, it can be applied only outside of the bifurcation point. At closer separations, only the SDI technique can be used.

5. ROLE OF IFS AND APPLICATIONS

5.1 Planet detection

SPHERE is expected to achieve better contrast that presently available instruments by about two orders of magnitude. This would imply a large improvement in mass limits. The smallest planets detectable with SPHERE have masses below 1 M_j, which represents an order of magnitude improvement over current detections or upper limits. Not only SPHERE will detect planets over a wide range of masses, but it will also be able to provide an unbiased distribution with masses over a reasonably wide mass range. This is possible exploiting young targets.

But on of the most powerful features of SPHERE is the possibility to explore a wide range of separations from the central star, which is allowed by combining IFS (very deep observations in the central region) and IRDIS (wide sky

coverage). This allows a nearly constant limiting contrast over a wide area, strongly enhancing the capability to derive useful information on the distribution of planets with semi-major axis, a crucial issue in models for formation of planetary systems.

A summary of data obtained by Monte Carlo simulation is given in Tab. 3. 60-70% of planets should be detected by both channels. This is useful for detection confirmation and false alarms rejection. About 20-25% should be detected by IFS only. These are planets detected in the inner regions thanks to the superior performances of IFS. About 5-20% of planets (highly dependent on the actual separation distribution of planets) should be detected by IRDIS only in the outer regions. These simulations confirm the synergy and complementarities between the two NIR instruments of SPHERE.

The number of planets expected to be detected is a very strong function of the (assumed) distribution of planet separation. Extending the semi-major axis distribution up to P=250 yr (about 40 AU) yield a number of planet detections about 3.5 larger than for the same distribution truncated at P=70 yr (about 17 AU). Several tens of planet detection (details depend on target number and selection criteria) are then expected between 20 and 40 AU if planets are there. SPHERE has clearly the potential for an accurate determination of the frequency of planets in wide orbits. Note that while giant planets are not expected to be found in large number at very wide separation (a>50-100 AU), brown dwarfs might instead be present. These objects represent an additional niche for IRDIS at wide separation from the central star

Tab. 1. Expected planet detections with IFS and IRDIS. The absolute numbers depend sensitively on the adopted target list and normalization adopted in the Monte Carlo simulation.

	% of detected planets	N Planets	% of detected planets	N Planets
	Distribution extended up to P<70 yr		Distribution extended up to P<250 yr	
IFS+IRDIS	73%	19.5	62%	57.8
IFS	21%	5.7	17%	15.7
IRDIS only	6%	1.6	21%	19.5
Total		26.7		93.1

5.2 Planet Characterization

To fully characterize the new discovered planets (e.g. temperature, chemical composition of the atmosphere, etc.), it should be important to be able to reconstruct their spectra at a good fidelity level.

To this aim we developed a pipeline in order to analyze data on the calibrated datacube resulting from our simulations. The datacube in our case is composed by 33 images at different wavelengths for the J-mode (λ=0.95-1.35 μm) and by 38 images for the J+H-mode (λ=0.95-1.70 μm). The procedure is composed by different steps:

- Speckle noise subtraction from the original datacube using the spectral deconvolution algorithm.

- Summing all the resulting images to create a single multi-wavelength image

- Search for objects on the summed image

- Extraction of a spectrum for every object found

- Spectral classification of every object through a cross-correlation with template spectra

To test the capability of our procedure to find and to correctly classify the extrasolar planets we did a series of simulations using a simulation code (CSP[2]) developed to simulate the performances of the IFS. In these simulations we introduce several extra solar planets at different separations (0.3, 0.5 and 1.0 arcsec) and with different contrasts (10^{-5}, 3×10^{-6}, 10^{-6} and 3×10^{-7}) respect to the central star. In order to test the capability of our procedure to correctly classify the

found objects, the input spectra of the simulated companion objects were of different types (T7, T2, L8, L0 and M2). In each simulations we have 5 different simulated objects at the same separation from the central star. In order to avoid crowding effects in the 0.3 arcsec case only 2 simulated planets instead of 5 have been introduced. In Figure 9 we display a series of multi-wavelength images obtained from different T7 input spectra simulations.

From the simulation performed we found almost all the simulated objects (90% in the J-mode and 95% in the J+H-mode). As expected, as the spectral classification was better for objects at greater separations from the central star and with higher luminosity contrast. Moreover better results were obtained with late spectral types object. I.e. T7 objects are generally correctly classified while for T2 and L8 we have a spread over a larger number of spectral types and L0 are generally seen as M8 type. We test the capability of our method to correctly disentangling the effects of the gravity using as input two different synthetic spectra with log(g) =4.0 and 5.5 and the same temperature (800 K). We conclude that using the J+H-mode we should be able to distinguish between the two different case while this should not be possible with the J-mode.
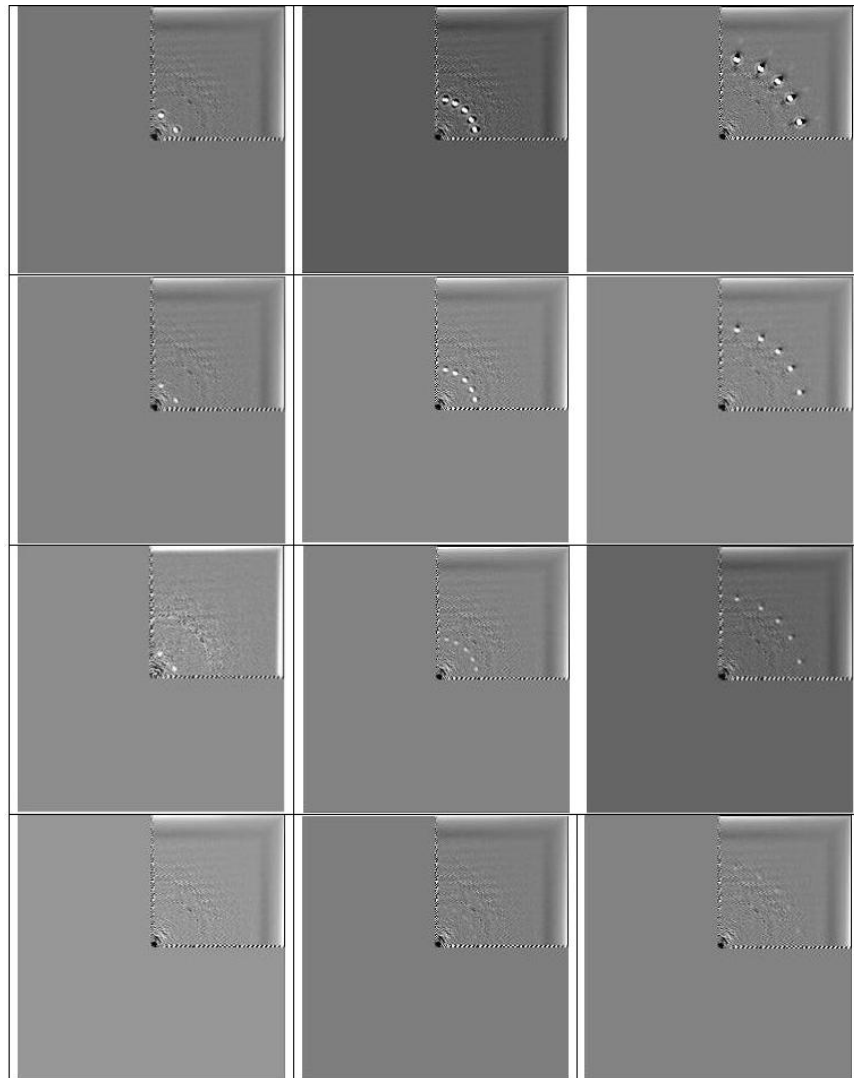

Figure 9 - Final multi-wavelength images obtained for simulations of the J-mode at different contrast (0.3, 0.5 and 1.0 arcsec from left to right) and with different contrasts respect to the central star (10^{-5}, 3×10^{-6}, 10^{-6} and 3×10^{-7} from top to bottom) with a T7 spectral type input spectrum

After virtual world we test our procedure in a more realistic case simulating the detection of companion objects around β-Pictoris. In this case we used as input the synthetic spectra of planets with 1, 5, and 10 M_{jup} at the usual separations. In this case the contrast for the central star has been calculated to be 3.70×10^{-7}, 1.35×10^{-5} and 1.03×10^{-4} for the three considered cases respectively. Like for the previous simulations we are able to find almost all the simulated objects. In general the 1 M_{jup} objects are classified as late type T spectral type, the 5 M_{jup} objects as early type T (with greater spread respect to the previous case) and the 10 M_{jup} is classified as M8 or L1 spectral type.

Finally to test the possibility of false alarm given by the presence of stellar contaminant in the instrument FOV we made simulations under the same conditions of the β-Pictoris ones but using as input K4V and M8V spectra. In this case we are able to correctly spectrally classify the M8 case while the K4 case is generally identified as M4 or M8 (our method does not seem to work very well for flat spectra). However it is important to stress the fact that in non case the contaminant objects are identified as L or T spectral type.

6. CONCLUSION

Integral Field Spectroscopy represents a powerful instrument for the detection and characterization of EGPs with constrast values both in the realm of (young) Jupiter-like planets, i.e. the main target of the IFS channel of SPHERE, and in the realm of the Earth-like planets, i.e. the cornerstone of this field of research in Astrophysics.

The purpose of high contrast diffraction limited Integral Field Spectroscopy is to exploit all the spectral features proper of EGPs atmosphere, in order to perform what - throughout this overview - is indicated as an improvement of the standard Simultaneous Differential Imaging, the Spectroscopic Simultaneous Differential Imaging. Moreover, by Integral Field Spectroscopy is possible to extract the spectrum of the candidate EGPs, retaining both continuum and spectral features, by adopting the extension of the Spectral de-convolution technique on the final 3D data cube.

Inside the SPHERE project, the Integral Field Spectroscopy channel is conceived in order to realize the S-SDI calibration technique, and at least in few cases, to get the spectrum of the candidate EGPs and characterize them.

REFERENCES

[1] J. Antichi, K. Dohlen, R. Gratton, D. Mesa, R. Claudi, E. Giro, A. Boccaletti, D. Mouillet, P. Puget, J.L. Beuzit, "BIGRE: a low cross-talk integral field unit tailored for Extrasolar Planets imaging spectroscopy", ApJ, 645-2, 1042, (2009)
[2] A. Berton, R. G. Gratton, M. Feldt, S. Desidera, E. Masciadri, M. Turatto, R. U. Claudi, G. Piotto, C. Pernechele, and J. Antichi, "Simulations of exoplanets detection obtained with a high-contrast imaging instrument: CHEOPS", Proc. SPIE 5490, 672 (2004)
[3] C. Marois, D. Lafrenière, R. Doyon, B. Macintosh, D. Nadeau, "Angular Differential Imaging: A Powerful High-Contrast Imaging Technique", ApJ, 641, 556, (2006)
[4] D. Lafreniere, R. Doyon, D. Nadeau, E. Artigau, C. Marois, M. Beaulieu," A New Algorithm for Point-Spread Function Subtraction in High-Contrast Imaging: A Demonstration with Angular Differential Imaging", ApJ, 660, 770, (2007)
[5] C. Marois, R. Doyon, R. Racine, D. Nadeau, "Efficient Speckle Noise Attenuation in Faint Companion Imaging", PASP, 112, 91 (2000)
[6] C. Marois, D. W. Phillion, B. Macintosh, "Exoplanet detection with simultaneous spectral differential imaging: effects of out-of-pupil-plane optical aberrations", , SPIE, 6269, 114 (2006)
[7] W.B. Sparks, H.C. Ford, " Imaging Spectroscopy for Extrasolar Planet Detection", ApJ, 578, 543, (2002)
[8] N. Thatte, R. Abuter, M. Tecza,E.L. Nielsen, F.J. Clarke, L. M. Close, "Very high contrast integral field spectroscopy of AB Doradus C: 9-mag contrast at 0.2arcsec without a coronagraph using spectral deconvolution", MNRAS, 378, 1229, (2007)